JLab PAC12 Proposal Cover Sheet

Jefferson Lab
User Liaison Office, Mail Stop 12 B
12000 Jefferson Avenue
Newport News, VA 23606

(Choose one)

☒ New Proposal Title: Measurement of $F_{\gamma^*\gamma\pi^0}$ at Low Q^2 via the Virtual Primakoff Effect

☐ Update Experiment Number:

☐ Letter-of-Intent Title:

Contact Person

Name: Daniel S. Dale
Institution: University of Kentucky
Address: Department of Physics and Astronomy
Address: 177 Chemistry/Physics Building
City, State, ZIP/Country: Lexington, KY 40506
Phone: 606-257-2504 Fax: 606-323-2846
E-Mail: DALE@pa.uky.edu

Experimental Hall: A Days Requested for Approval: 10

Jefferson Lab Use Only

Receipt Date: 6/26/97 97-009

By:

Lab Proposal No.: _____ Date: _____

.ll: A Anticipated Run Date: _____ PAC Approved Days: _____

;pokesperson: Dan Dale
'hone: 606-257-2504
:-mail: DALE@pa.uky.edu

Hall Liaison: _____

List all combinations of anticipated targets and beam conditions required to execute the experiment. (This list will form the primary basis for the Radiation Safety Assesment Document (RSAD) calculations that must be performed for each experiment.)

Condition No.	Beam Energy (MeV)	Mean Beam Current (μA)	Polarization and Other Special Requirements (e.g., time structure)	Target Material (use multiple rows for complex targets — e.g., w/windows)	Material Thickness (mg/cm²)	Est. Beam-On Time for Cond. No. (hours)
1	6000	5	none	Pb	6.35	240

The beam energies, E_{Beam}, available are: $E_{Beam} = N \times E_{Linac}$ where N = 1, 2, 3, 4, or 5. E_{Linac} = 800 MeV, i.e., available E_{Beam} are 800, 1600, 2400, 3200, and 4000 MeV. Other energies should be arranged with the Hall Leader before listing.

LAB RESOURCES LIST

JLab Proposal No.: _____ Date June 26, 1997

(For JLab ULO use only.)

List below significant resources — both equipment and human — that you are requesting from Jefferson Lab in support of mounting and executing the proposed experiment. Do not include items that will be routinely supplied to all running experiments such as the base equipment for the hall and technical support for routine operation, installation, and maintenance.

Major Installations *(either your equip. or new equip. requested from JLab)*

Lead glass detectors with support structure to be mounted upstream of Hall A möller polarimeter dipole. Cherenkov and wire chamber detectors.

New Support Structures: 1) For lead glass 2) wire chambers 3) Cherenkov

Data Acquisition/Reduction

Computing Resources: _____

New Software: _____

Major Equipment

Magnets: _____

Power Supplies: _____

Targets: _____

Detectors: _____

Electronics: _____

Computer Hardware: _____

Other: _____

Other: _____

HAZARD IDENTIFICATION CHECKLIST

JLab Proposal No.: _____ Date: _____
(For CEBAF User Liaison Office use only.)

Check all items for which there is an anticipated need.

Cryogenics
- _____ beamline magnets
- _____ analysis magnets
- _____ target
  - type: _____
  - flow rate: _____
  - capacity: _____

Electrical Equipment
- _____ cryo/electrical devices
- _____ capacitor banks
- _____ high voltage
- _____ exposed equipment

Radioactive/Hazardous Materials
List any radioactive or hazadorous/ toxic materials planned for use:
_____
_____
_____
_____

Pressure Vessels
- _____ inside diameter
- _____ operating pressure
- _____ window material
- _____ window thickness

Flammable Gas or Liquids
- type: _____
- flow rate: _____
- capacity: _____

Drift Chambers
- type: MwPc
- flow rate: 2 liters/hour
- capacity: 4 liters

Other Target Materials
- ___ Beryllium (Be)
- ___ Lithium (Li)
- ___ Mercury (Hg)
- ___ Lead (Pb)
- ___ Tungsten (W)
- ___ Uranium (U)
- ___ Other (list below)

_____
_____

Vacuum Vessels
- _____ inside diameter
- _____ operating pressure
- _____ window material
- _____ window thickness

Radioactive Sources
- _____ permanent installation
- _____ temporary use
- type: _____
- strength: _____

Large Mech. Structure/System
- _____ lifting devices
- _____ motion controllers
- _____ scaffolding or
- _____ elevated platforms

Lasers
- type: _____
- wattage: _____
- class: _____

Installation:
- _____ permanent
- _____ temporary

Use:
- _____ calibration
- _____ alignment

Hazardous Materials
- ___ cyanide plating materials
- ___ scintillation oil (from)
- ___ PCBs
- ___ methane
- ___ TMAE
- ___ TEA
- ___ photographic developers
- ___ other (list below)

_____
_____

General:

Experiment Class:

- _____ Base Equipment
- _____ Temp. Mod. to Base Equip.
- _X_ Permanent Mod. to Base Equipment
- _____ Major New Apparatus

Other: _____
_____

Measurement of $F_{\gamma^*\gamma\pi^0}$ at Low Q^2 via the Virtual Primakoff Effect

D. Dale (co-spokesperson and contact person), B. Doyle,
A. Gasparian (co-spokesperson), T. Gorringe, W. Korsch,
M. Kovash, V. Zeps
University of Kentucky, Lexington, KY

A. Afanasev, J.P. Chen, D. Mack, J. Mitchell, S. Nanda, A. Saha, B. Wojtsekhowski
TJNAF, Newport News, VA

A. Glamazdin, V. Gorbenko, A. Omelaenko, R. Pomatsalyuk
Kharkov Institute of Physics and Technology, Kharkov, Ukraine

Rory Miskimen
University of Massachusetts, Amherst, MA

Adam Sarty
Florida State University, Tallahassee, FL

A. Margarian
Yerevan Physics Institute, Yerevan, Armenia

S. Danaguolian
North Carolina A&T State University, Greensboro, NC

Members of the Hall A Collaboration are invited to participate.

Abstract

We propose to measure the neutral pion form factor $F_{\gamma^*\gamma\pi^o}$ at low Q^2 using small angle electroproduction of π^o's in the Coulomb field of a heavy nucleus. These measurements will provide fundamental information on the interaction radius of the pion in the $\gamma^*\gamma\pi^o$ transition. Such low Q^2 measurements are expected to be largely model independent in their extraction of this interaction radius, as they are quite insensitive to the functional form used for the form factor in its extrapolation to the photon point. This experiment will utilize the unique small scattering angle capabilities of the TJNAF Hall A Möller polarimeter.

Introduction

As an ingredient in theories of few-body and heavy nuclei and as a fundamental testing ground for QCD, the properties of the pion have generated intense interest. The structure of the pion's electromagnetic coupling is typically studied in the context of the vector meson dominance model in which a photon couples to hadronic matter via an intermediate vector meson. Such a model implies a form factor of the form:

$$F_\pi = \frac{1}{1 + q_\mu^2/m_\rho} \approx 1 - < r^2 > \frac{q_\mu^2}{6}, \tag{1}$$

where m_ρ is the mass of the ρ meson, and the approximation holds at low q_μ^2. For the charged pion case, the Coulomb form factor has been measured[1] and the charge radius was determined to be about 0.6 fm. Due to charge conjugation symmetry, however, the elastic Coulomb form factor ($\gamma\pi^o\pi^o$) vanishes. The $\gamma^*\gamma\pi^o$ transition vertex, on the other hand, is of great interest and has been studied theoretically from the point of view of models based on the VDM as well as those involving treatments of the π^o quark substructure[2][3]. This transition is characterized by the form factor $F(q_1^2, q_2^2)$ which, if only one photon has significant mass, depends upon a form factor typically parameterized by the pole form (1), and approximated at low q_μ^2 by:

$$F_{\gamma^*\gamma\pi^o} \approx 1 - a\frac{q_\mu^2}{m_\pi^2}. \tag{2}$$

where a is a measure of the $\gamma^*\gamma\pi^o$ interaction radius.

Previous experiments in the time-like region

A number of experiments aimed at measuring a have been performed in the time-like momentum transfer region utilizing the π^o Dalitz decay $\pi^o \rightarrow e^+e^-\gamma$ reaction[3-12] The amplitude for this process involves the $F_{\gamma^*\gamma\pi^o}$ form factor which, in the usual linear expansion

$$F(x) \approx 1 + a\frac{m_{e^+e^-}^2}{m_{\pi^o}^2}. \tag{3}$$

a	reference
$+0.025 \pm 0.014 \pm 0.026$	Meijer Drees, 1992 [4]
$+0.026 \pm 0.024 \pm 0.048$	Farzanpay, 1992 [5]
$-0.11 \pm 0.03 \pm 0.08$	Fonvielle, 1989 [6]
$-0.01 + 0.08 - 0.06$	Gumplinger, 1987 [7]
$0.12 + 0.05 - 0.04$	Tupper, 1983 [8] (reanalysis of [9])
$+0.10 \pm 0.03$	Fischer, 1978 [9]
$+0.02 \pm 0.1$	Burger, 1972 [10]
$+0.01 \pm 0.11$	Devons, 1969 [11]
-0.24 ± 0.16	Samios, 1961 [12]
-0.15 ± 0.10	Kobrak, 1961 [13]

A summary of these measurements is shown in the table above, where it can be seen that the published values for the slope range from -0.24 to $+0.12$. Such experiments suffer from small kinematically accessible ranges and significant backgrounds, and they require large final-state radiative corrections. As such, these experiments have not been able to determine even the sign of the form factor slope.

Previous measurements in the space-like region

The CELLO collaboration at PETRA has measured $F_{\gamma^*\gamma\pi^o}$ in the space-like region at large momentum transfers using the reaction $e^+e^- \rightarrow e^+e^-\pi^o$[14]. In this experiment two photons are radiated virtually by the colliding e^+e^- beams. One of the virtual photons is close to real and the other has a larger q_μ^2 and is tagged by the detection of an e^+ or e^-.

Measurements were taken at momentum transfers ranging from 0.62 to 2.17 $(GeV/c)^2$, and the value of a was deduced by extrapolation under the assumption of vector meson dominance. The authors quote a value of $a = 0.0325 \pm 0.0026$ (statistical) with systematic errors estimated to be of the same order as the statistical error. The results of these measurements are shown in figure 1 with the corresponding fit to $F_{\gamma^*\gamma\pi^o}$. New data covering the q_μ^2 region from 2 to 20 GeV^2 have also been reported by the CLEO collaboration[15]. In the experiment proposed here, however, this form factor will be measured in the very low q_μ^2 regime ranging from 0.01 to about 0.035 $(GeV/c)^2$ to extract a. Such studies will complement the higher q_μ^2 data from CELLO and CLEO. Measurements at extremely low q_μ^2 can be expected to greatly minimize the model dependency of the extraction of a, as they do not suffer from the large systematic uncertainties associated with the extrapolation to $q_\mu^2 \rightarrow 0$.

The proposed experiment

The real Primakoff effect on heavy nuclei has been used in a number of experiments to study the π^o[16][18][19]. The production of π^o's in the Coulomb field of a nucleus by real photons is essentially the inverse decay $\pi^o \rightarrow \gamma\gamma$, and the cross section for this process thus provides a measure of the pion lifetime. In 1989, Hadjimichael and Fallieros[20] suggested that the virtual Primakoff effect, figure 2, could access additional fundamental information about the pion as the cross section is proportional to $|F_{\gamma^*\gamma\pi^o}(q_\mu^2)|^2$. The full expression for the virtual Primakoff scattering cross section is[20][21]:

$$\frac{d^3\sigma}{d\epsilon_2 d\Omega_2 d\Omega_\pi} = \frac{Z^2\eta^2}{\pi}\sigma_M \frac{Q^4}{K^4}\frac{\beta_\pi^{-1}}{\omega_\pi}|F_N(K^2)|^2|F_{\gamma^*\gamma\pi^o}(q_\mu^2)|^2 sin^2(\frac{\theta_e}{2})sin^2(\theta_\pi)[4\epsilon_1\epsilon_2 sin^2\phi_\pi + |\vec{q}|^2/cos^2(\frac{\theta_e}{2})] \quad (4)$$

where σ_M is the Mott cross section, $\eta^2 = (4/\pi m^3)/\tau$, τ is the π^o lifetime, K is the (nearly real) photon four momentum from the Coulomb field, the pion four momentum is $Q = (\vec{q}, \omega_\pi)$, $\beta_\pi = \vec{q}/\omega_\pi$, and $F_N(K^2)$ is the nuclear form factor.

As can be seen from the above expression for the form factor (1), the sensitivity to a (or equivalently to the interaction radius) calls for a finite value of q_μ^2 whereas the cross section is larger at lower q_μ^2. Hadjimichael and Fallieros examined the sensitivity of the cross section to a for energy transfers up to 1.6 GeV. They saw only moderate sensitivity and noted that the cross section is optimized for $\theta_e \rightarrow 0$ and $\theta_\pi \rightarrow 0$ whereas pion energies above 2 GeV are favored for probing the $\gamma^*\gamma\pi^o$ vertex. We have extended these calculations to kinematical regimes available with the 6 GeV electron beam at TJNAF and the Hall A Möller polarimeter, *i.e.* to θ_e of 2.7 degrees and energy transfers of 4.4 GeV, and note that good sensitivity to the $\gamma^*\gamma\pi^o$ form factor is present.

Figure 3 shows the cross sections for the virtual Primakoff process on lead for a fixed electron energy loss of 4.4 GeV, and electron scattering angle of 2.7 degrees and a pion angle of 0.1 degrees with respect to $\vec{q}$. The two curves are for the VDM prediction ($a = 0.03$) and that determined by the $\pi^o \rightarrow e^+e^-\gamma$ experiment ($a = 0.1$) of reference [9]. From the plot one can see that the cross sections are large, and are quite sensitive to the pion transition form factor. If we define a figure of merit to be the difference in the predicted cross section for the two form factors times the square root of the average cross section, figure 4, we see that the optimal kinematics are at θ_e=1 - 3 degrees and $\omega \approx 4$ GeV. While such kinematics are difficult to access with most standard electron spectrometer systems, the TJNAF Hall A Möller polarimeter is uniquely suited for such very small angle electron scattering measurements.

The TJNAF Hall A Möller Polarimeter

As part of the spin physics program at TJNAF, the University of Kentucky, the Kharkov Institute of Physics and Technology, and TJNAF are developing a Möller polarimeter for Hall A. This electron polarimeter will be a part of the standard beamline instrumentation and its principle design requirements are as follows:

- high counting rate and high precision ($\Delta p \approx 3\%$) for the polarization measurement,
- fixed element positions within the whole energy range (0.8 – 6 GeV),
- large signal-to-background ratio,
- minimum perturbations on the beam parameters and trajectory.

The device will use electron-electron (Möller) scattering in a set-up in which the polarized electron beam is scattered from a polarized electron target. The asymmetry obtained in the scattering for the case in which the electron spins are aligned *versus* anti-aligned gives the polarization of the incident electron beam. A set of magnets and particle detectors will analyze the kinematics of the scattered electrons. The polarimeter can be divided into the following sub systems (see figure 5):

- A polarized electron target,
- Three quadrupole magnets for selection of the angular range of the Möller electrons,
- A dipole magnet for energy analysis of the Möller electrons,
- The detectors for the Möller electrons.

A top view of the layout of the polarimeter is shown in figure 5. Polarized electrons from the TJNAF accelerator are incident upon a magnetized iron foil which serves as the polarized electron target. Pairs of electrons which have undergone Möller scattering exit the target and are focussed in a series of three quadrupole magnets. Since the analyzing power for Möller scattering is maximum for scattering at 90 degrees in the center of mass system, the optics are chosen to select electrons which each have half the incident beam energy and have symmetric angles with respect to the beam. The optimum Möller angles are dependent upon the incident beam energy and range from 0.75 to 2.3 degrees. The quadrupoles transform the trajectories of the Möller electrons such that they become parallel to the incident beam. They are then momentum analyzed in a dipole magnet (bent into the page in the figure) and detected, in coincidence, by a set of lead glass and plastic detectors. In order to not perturb the main electron beam as it passes through the dipole, a piece of iron is placed

on the median plane of the dipole with a hole drilled along its length to accommodate the beam. This provides magnetic shielding for the electron beam so that it may pass through the dipole without deflection.

Experimental considerations

With some relatively minor modifications, this device can be used to measure the $(e, e'\pi^o)$ cross section at low q_μ^2. Principle backgrounds to the Primakoff mechanism will consist of nuclear coherent pion production and multiple pion production. The Primakoff cross section is zero for pions emmitted along $\vec{q}$, has a sharp maximum at an angle $\theta_\pi \sim m_\pi/2E_\pi^2$, and falls rapidly to zero at larger angles. It is proportional to Z^2 and its peak value is roughly proportional to E^4. The nuclear coherent cross section is also zero in the forward direction, has a broad maximum outside the angular region of the Primakoff effect, and falls at larger angles as shown in figure 6. It is expected to vary little with energy[17]. Consequently, this experiment requires a π^o detector with good angular resolution to eliminate nuclear coherent production and modest energy resolution will enable an invariant mass cut to suppress multi photon backgrounds. To carry out such a measurement, we propose to remove the third polarimeter quadrupole magnet and move the first and second quadrupoles to positions 44.5 and 93.9 cm downstream of the Möller target position, respectively. In addition, we plan to place a series of lead glass photon detectors just upstream of the dipole. With minor modifications to the vacuum system, one can registrate the two photons from the decay of the π^o's and, using the first two Möller polarimeter quadrupole magnets, focus the scattered electrons on the Möller polarimeter detector package. A GEANT generated invariant mass distribution from such an experimental geometry is shown in figure 7. A series of four arrays of lead glass detectors are proposed as shown in figure 8 which shows a side view of the modified Möller polarimeter along with a GEANT simulation of one virtual Primakoff event. For these kinematics, the photons come out at about 2 degrees with respect to the pion.

Position resolution in the lead glass photon detectors is required to constrain $\theta_{\pi^o\vec{q}}$ to small angles (less than about one degree) to exclude nuclear coherent pion production. A GEANT generated simulation of the $\theta_{\pi^o\vec{q}}$ resolution for a 3×3 array of $4 \times 4 \times 40$ cm lead glass blocks is shown in figure 9, where the angular resolution is found to be about 0.5 degrees. Simple estimates[22] indicate that by choosing $|t| < 2 \times 10^{-4}(GeV/c)^2$, the Primakoff mechanism dominates over ρ^o and ω exchanges in the t-channel. Typical $|t|$'s for the kinematics suggested here are around $5 \times 10^{-5}(GeV/c)^2$.

At the kinematics under consideration here, the opening angle of the π^o decay photons is about 4 degrees, and the pion angle is about one degree with respect to the beam. The most favored location for the lead glass blocks is 3 meters downstream of the target and about twelve centimeters from the beam. A series of plastic veto detectors in front of the

lead glass blocks will be employed to reject charged particles.

Count rate estimates

Due to the high flux of virtual photons at small electron scattering angles, the cross sections for this process are relatively high. On the other hand, the backgrounds in the π^o detector argue for low beam currents and a thin target. Count rates estimates were performed for θ_e=2.7 degrees, incident electron beam of 5μA and energy of 6 GeV and a lead target with a thickness of 10^{-3} radiation lengths. Acceptances for the electron arm were calculated from the Möller polarimeter optics with a series of four lead glass detectors placed just upstream of the Möller dipole. The sensitivity to the form factor $F_{\gamma^*\gamma\pi^o}$, with projected error bars obtained as described below, is shown in figure 10. It should be noted that the maximum q_μ^2 is limited by the focusing ability of the first two Möller quadrupole magnets and the incident beam energy. In this regard, the higher the available beam energy, the more favorable the lever arm is for determining a. The lower q_μ^2 points on the other hand, extend the lever arm for determination of the slope of the form factor, and provide a check of the systematic errors in ensuring that the form factor extrapolates back to 1 at low q_μ^2. Whereas relative cross section measurements are adequate for determining the slope of $F_{\gamma^*\gamma\pi^o}$, absolute cross sections enable one to use the known value at $q_\mu^2 = 0$ to constrain the slope. As such, we intend to obtain absolute cross sections.

On the electron arm, count rates estimates were performed for the virtual Primakoff effect, for (e,π^-) using the code EPC of Lightbody and O'Connell, and for inclusive (e, e^-) processes using the code QFS also of Lightbody and O'Connell[23]. The results are shown in the accompanying table.

The kinematics for Möller scattering of a 6 GeV beam lie outside the energy and angle ranges of the Möller spectrometer (see figure 11), and therefore are not expected to contribute significantly to the electron rates. The π^- rates indicate the need for a gas Cherenkov detector for particle identification. In addition, we propose the construction of a detector with coordinate resolution to enable adequate resolution in q_μ^2.

The following cross sections and acceptances were used in the count rate estimates. The rates quoted for the virtual Primakoff effect in the following table are integrated over all π^o kinematics. π^o detection efficiency was taken into account in the final coincidence rate calculations. The polarimeter has two collimators placed on the upstream side of the dipole magnet which can be used to define the acceptance in the azimuthal angle of the scattered electrons. In the rate estimates this acceptance was taken to be $\pm 5°$.

E' (GeV)	$\theta_{low} - \theta_{high}$ (degrees)	$\Delta\Omega_e$ (msr)	$(e,e')\pi^o$ $\mu b/(srMeV)$	(e,π^-) $\mu b/(srMeV)$	(e,e') $\mu b/(srMeV)$
1.6	1.9–3.2	0.35	4.2×10^{-4}	3.3×10^{-2}	2.9
1.7	1.7–2.6	0.21	5.3×10^{-4}	3.2×10^{-2}	4.2
1.8	1.5–2.2	0.14	9.1×10^{-4}	3.1×10^{-2}	6.0
1.9	1.4–2.0	0.11	9.1×10^{-4}	2.9×10^{-2}	7.4
2.0	1.35–1.9	0.095	1.3×10^{-3}	2.8×10^{-2}	8.8

We obtain the following rates for a 5μA beam current and a Pb target of thickness 10^{-3} radiation lengths. The $(e,e'\pi^o)$ coincidence rates were calculated with a 25% pion detection efficiency.

E' (GeV)	$(e,e')\pi^o$ counts/sec	$(e,e'\pi^o)$ coinc counts/day	(e,π^-) counts/sec	(e,e') counts/sec
1.6	8.5×10^{-3}	180	6.0×10^{-1}	58
1.7	6.5×10^{-3}	135	3.7×10^{-1}	50
1.8	7.0×10^{-3}	155	2.5×10^{-1}	48
1.9	5.5×10^{-3}	120	1.8×10^{-1}	46
2.0	6.5×10^{-3}	145	1.5×10^{-1}	47

The resulting projected error bars on $F_{\gamma\gamma^*\pi^o}$ are shown in figure 10.

Q^2 reconstruction

Figure 12 shows the range of q_μ^2 acceptance of the proposed experiment. As is evident from figure 11, a given scattered electron energy can arise from a range of scattered electron angles. Consequently, trajectory information must be measured to ensure adequate q_μ^2 resolution. Figure 13 shows the hit pattern of scattered electrons on the face of the present polarimeter detector package for two different scattered electron energies (1.62 GeV$\pm$0.5% and 1.69 GeV$\pm$0.5%) and two scattering angle ranges (each 1 mr in width with central values separated by 2 mr). The Y axis is the dispersive direction measured in centimeters from the beam. The X axis is also in centimeters and is the transverse direction measured from the median plane of the Möller dipole. Multiple scattering in the target and exit windows is

taken into account in the simulation. As is seen from the figure, the energies are separated in the dispersive direction, and the transverse direction is sensitive to the scattering angle. Figure 14 illustrates the typical expected resolution in q_μ^2 for a coordinate resolution of 4 mm.

The electron detector package

The present Möller polarimeter detector package is designed to measure two high energy electrons in coincidence. It consists of two sets each of an aperture plastic scintillation detector, a series of plastic scintillator hodoscope channels segmented in the dispersive direction, and some lead glass Cherenkov detectors (see figure 15). We plan to operate this detector package in its present configuration with an added gas Cherenkov detector for particle identification just upstream of the Möller detector package, and two U-V wire chambers (approximately 10 cm $\times$ 20 cm) in front of the gas Cherekov detector for trajectory definition.

π^o detection

The π^o's are produced with energies ω_π essentially equal to the energy transfer of the scattered electron, and are emmitted at angles very nearly along the three momentum transfer direction, which is directed about one degree with respect to the beamline. Figure 16 shows the spatial distribution of the π^o decay gamma rays as they propagate from the target to the π^o detector, with the final frame indicating the acceptance of the photon detectors. The present beampipe is shown for reference. To reduce secondary interactions in the beam pipe walls, we plan to enlarge the vacuum pipe downstream of the second quadrupole magnet up to the pion detector to accommodate both the scattered electrons and the pion decay photons, with a window just before the photon detectors for the photons to exit the vacuum. The gammas will actually describe two cones, each centered on the three momentum transfer direction corresponding to each electron arm of the polarimeter. Background neutral particle rates on the lead glass photon detectors were calculated with GEANT to be 2.5 kHz at 5μA with a 1 GeV threshold, and 25 kHz with a 1 MeV energy threshold.

Facility impact

We are requesting 10 days of beamtime in Hall A with an unpolarized 6 GeV (or highest energy available) beam at 5 μAmps. No energy or spectrometer angle changes are required. Since the necessary apparatus is largely decoupled from the Hall A High Resolution Spectrometers and targets, some or all of this program could conceivably be performed during what would otherwise be Hall A down time, such as in parallel with major equipment installation in the hall. Such an experiment would require an upgrade of the Möller polarimeter detector package so that it includes a gas Cherenkov detector and wire chambers. The Möller data aquisition system would have to modified to accommodate event mode data, and tem-

porary modifications to quadrupole positions and the vacuum system would need to be made.

The collaboration

By the time this experiment could run, many of the people involved in this collaboration will have had extensive experience with both the Hall A Möller polarimeter, and with running experiments at TJNAF. Many of us have been intimately involved in the design and construction of the polarimeter, and the collaboration includes a number of people who have extensive experience in designing and constructing the types of detectors needed to mount this experiment.

Summary

The TJNAF Hall A Möller polarimeter provides a unique opportunity to study physics in the extremely low q_μ^2 regime. In particular, a definitive, largely model independent measurement of the $\gamma^*\gamma\pi^o$ transition vertex which will provide fundamental information on the structure of the neutral pion is possible. The proposed hardware upgrades to the Hall A Möller polarimeter can be expected to open up the very low q_μ^2 regime to experimental investigation and to broaden the range of physics accessible at TJNAF.

References

[1] S.R. Amendolia et al., Phys. Lett. 146B (1984) 116.

[2] L.G. Landsberg, Phys. Rep. 128, no. 6 (1985) 302.

[3] M.A. Ivanov and V.E. Lyubovitskij, preprint number hep-ph/9705423, 1997.

[4] R. Meijer Drees et al., Phys. Rev. D, vol 45, no 5 (1992) 1439.

[5] F. Farzanpay et al., Phys. Lett. B 278 (1992) 413.

[6] H. Fonvieille et al. Phys. Lett. B 233 (1989) 65.

[7] P. Gumplinger, Doct. Thesis, Oregon State University (1987).; J.M. Poutissou et al., Proc. Lake Louise Winter Institute (1987), World Scientific, Singapore).

[8] G. Tupper et al., Phys. Rev. D, 28, no. 11 (1983) 2905.

[9] J. Fischer et al., Phys. Lett., vol 73B, no. 3 (1978) 359.

[10] J. Burger, Doct. Thesis, Columbia University (1972).

[11] S. Devons et al., Phys. Rev., vol. 184, no. 5 (1969) 1356.

[12] N.P. Samios, Phys. Rev. vol 121, no 1 (1961) 275.

[13] H. Kobrak, Il Nuovo Cimento, vol 20, no 6 (1961) 1115.

[14] H.J. Behrend, et al., Z. Phys C, 49 (1991) 401.

[15] V. Savinov (CLEO Collaboration), preprint number hep-ex/9507005, 1995.

[16] A. Browman et al., Phys. Rev. Letts. vol 33, no. 23 (1974) 1400.

[17] G. Bellettini et al., Il Nuovo Cimento, vol. 66, no. 1 (1970) 243.

[18] V.I. Kryshkin et al., Sov. Phys. JETP, vol. 30, no. 6 (1970) 1037.

[19] G. Bellettini et al., Il Nuova Cimento, vol 40, no. 4 (1965) 1139.

[20] E. Hadjimichael and S. Fallieros, Phys. Rev. C, vol. 39, no. 4 (1989) 1438.

[21] A. Omelaenko, Ukrainian Journal of Physics, vol 18, no. 8, (1973) 1249.

[22] Andre Afanasev, private communication, 1996.

[23] J.W. Lightbody and J.S. O'Connell, Computers in Physics (1988).

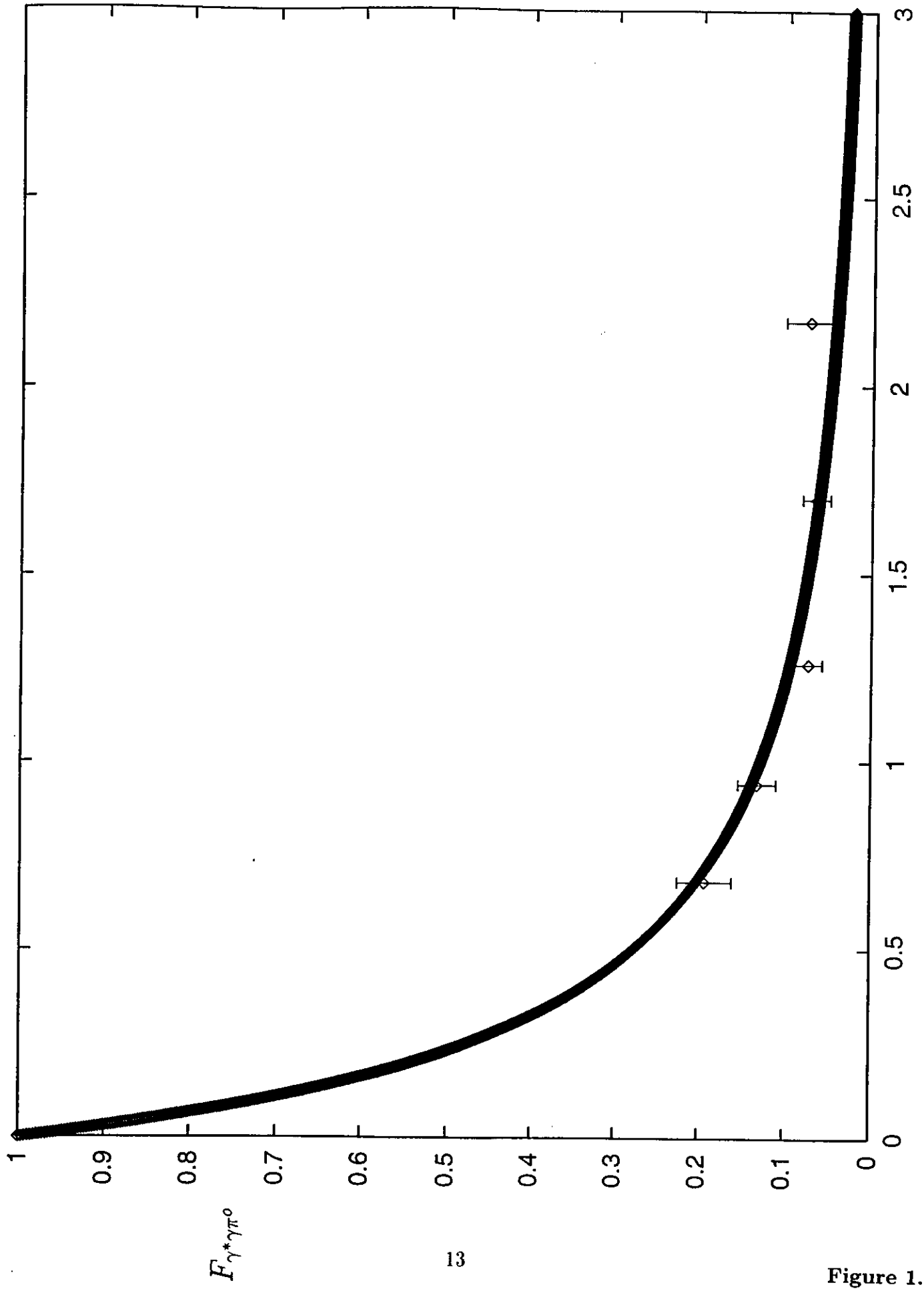

Figure 1.

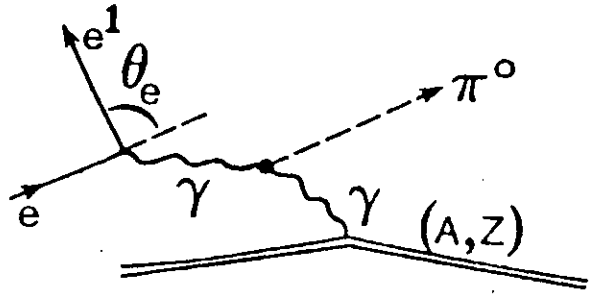

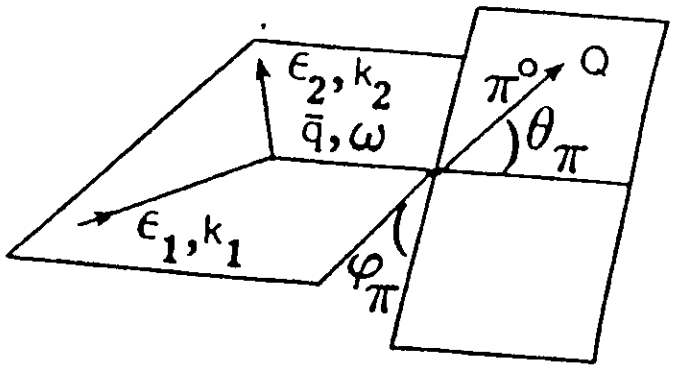

Figure 2. The virtual Primakoff process and its associated kinematics.

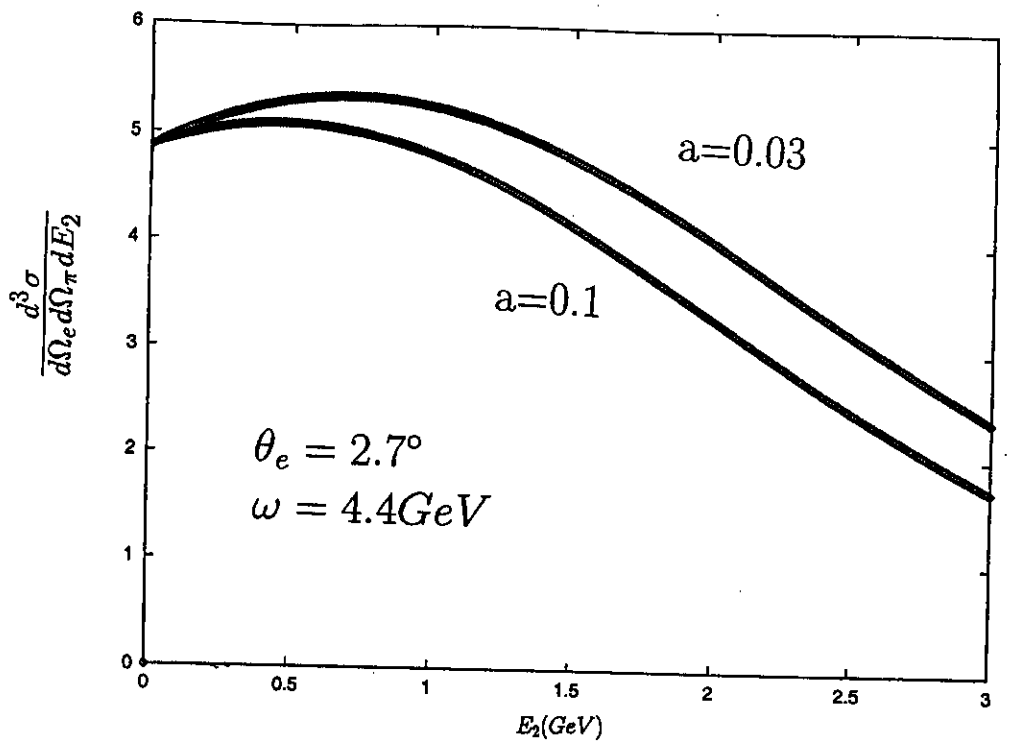

Figure 3. Cross sections *vs.* scattered electron energy.

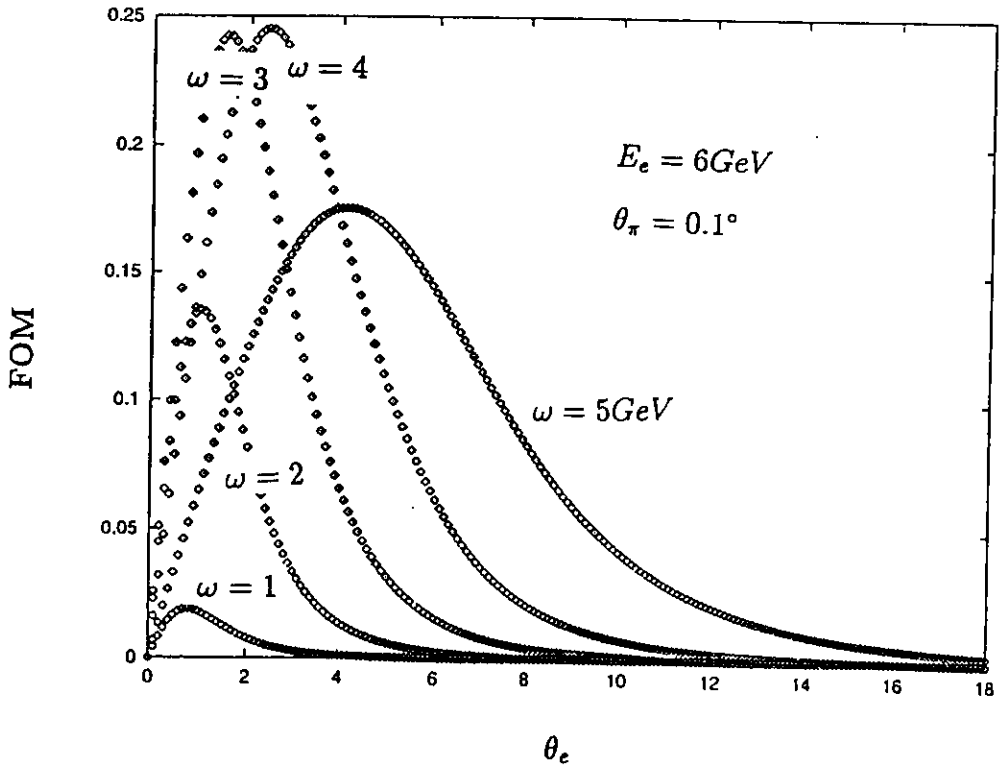

Figure 4. Figure of merit (see text) *vs.* electron scattering angle.

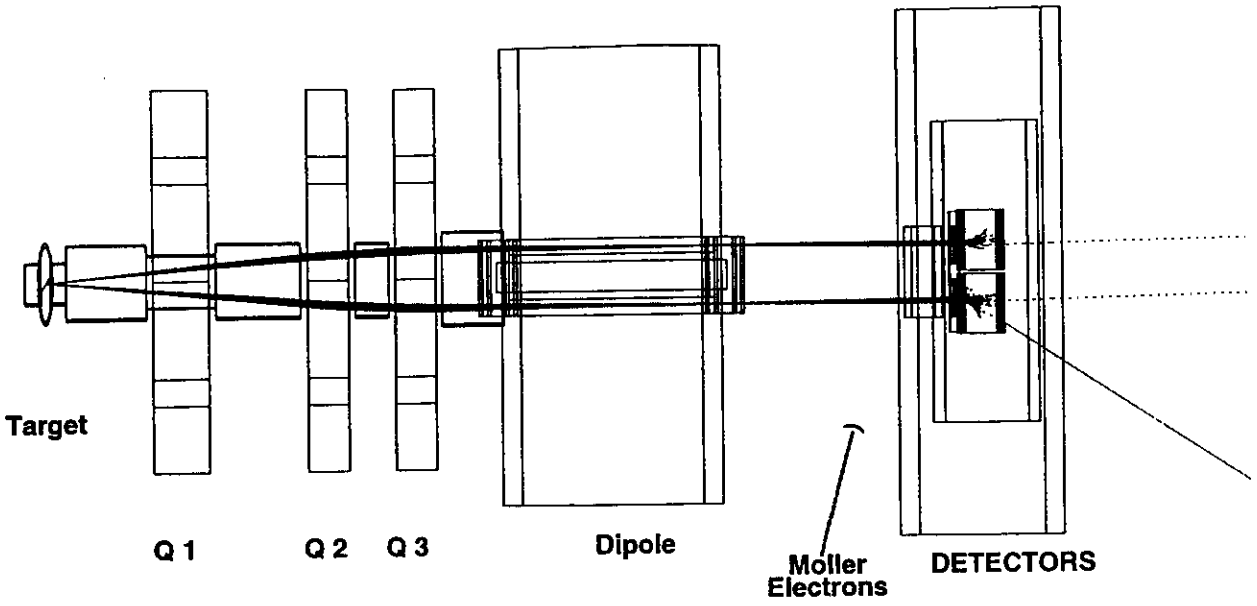

Figure 5. The TJNAF Hall A Möller Polarimeter.

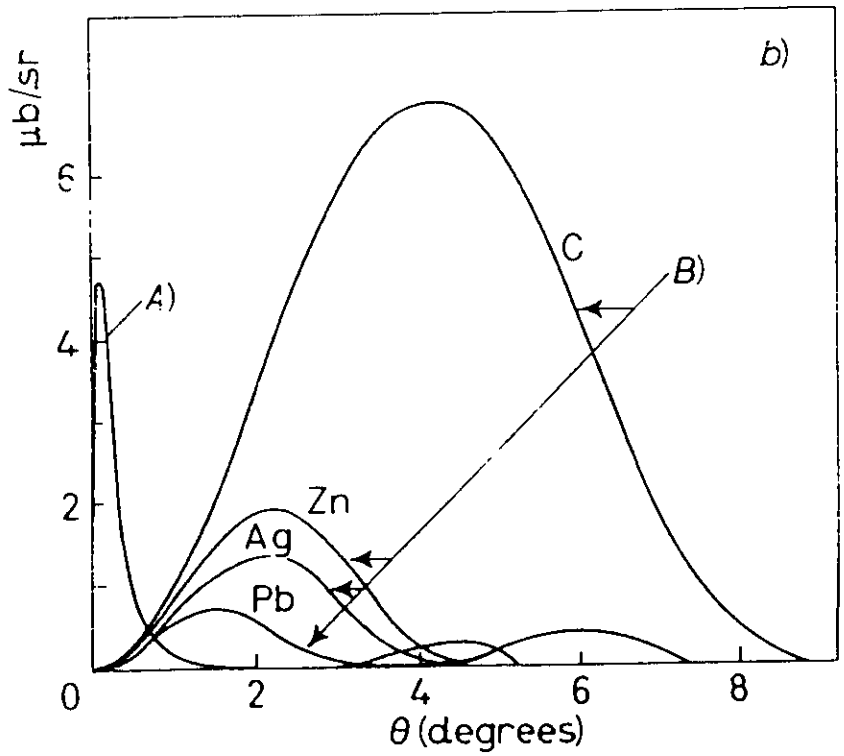

Figure 6. Curve A: Primakoff cross section divided by Z^2. Curve B: Nuclear coherent cross section divided by A^2. Photon energy is 2 GeV. Figure is from [17]. (Note: for the kinematics of this proposal, the ratio of the Primakoff to nuclear coherent peaks is approximately 16:1.)

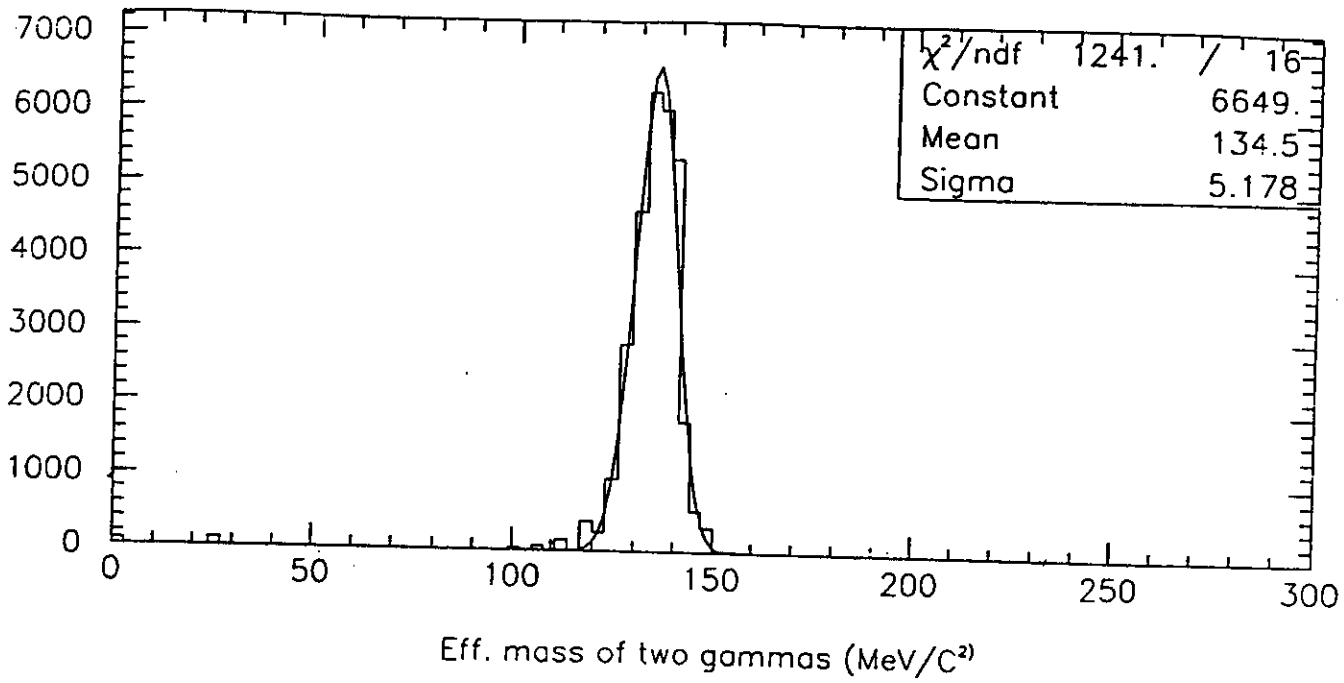

Figure 7. π^o invariant mass reconstruction.

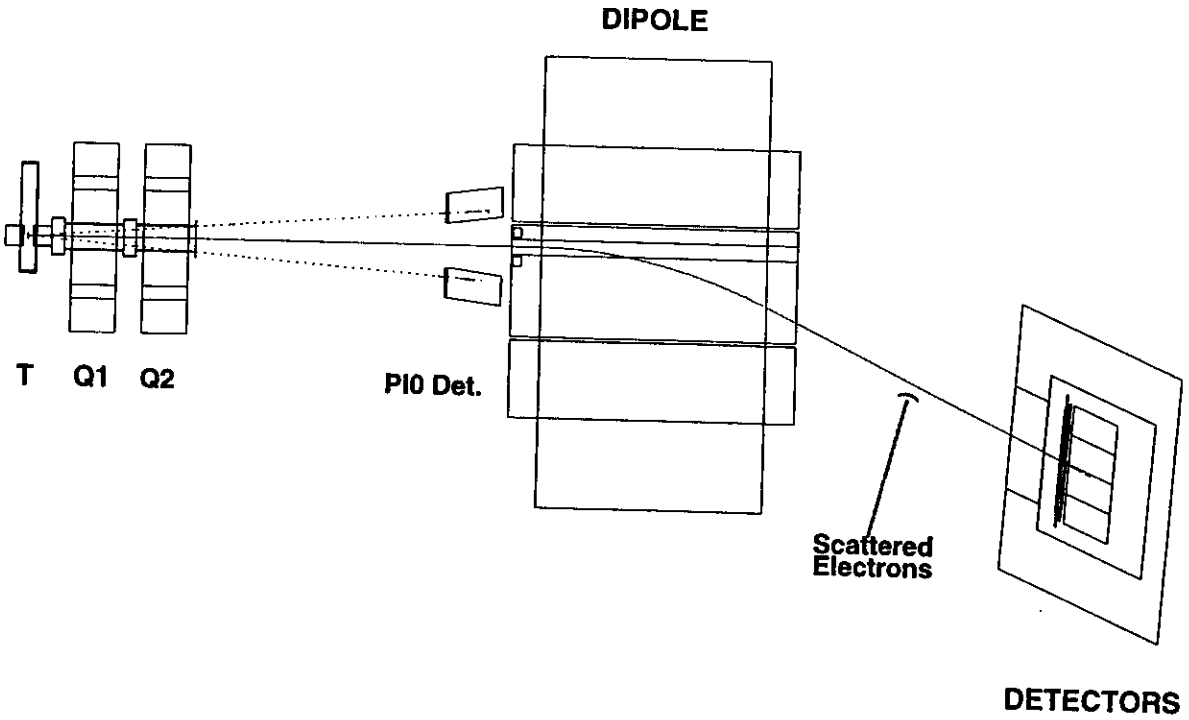

Figure 8. Side view of polarimeter with one virtual Primakoff event shown.

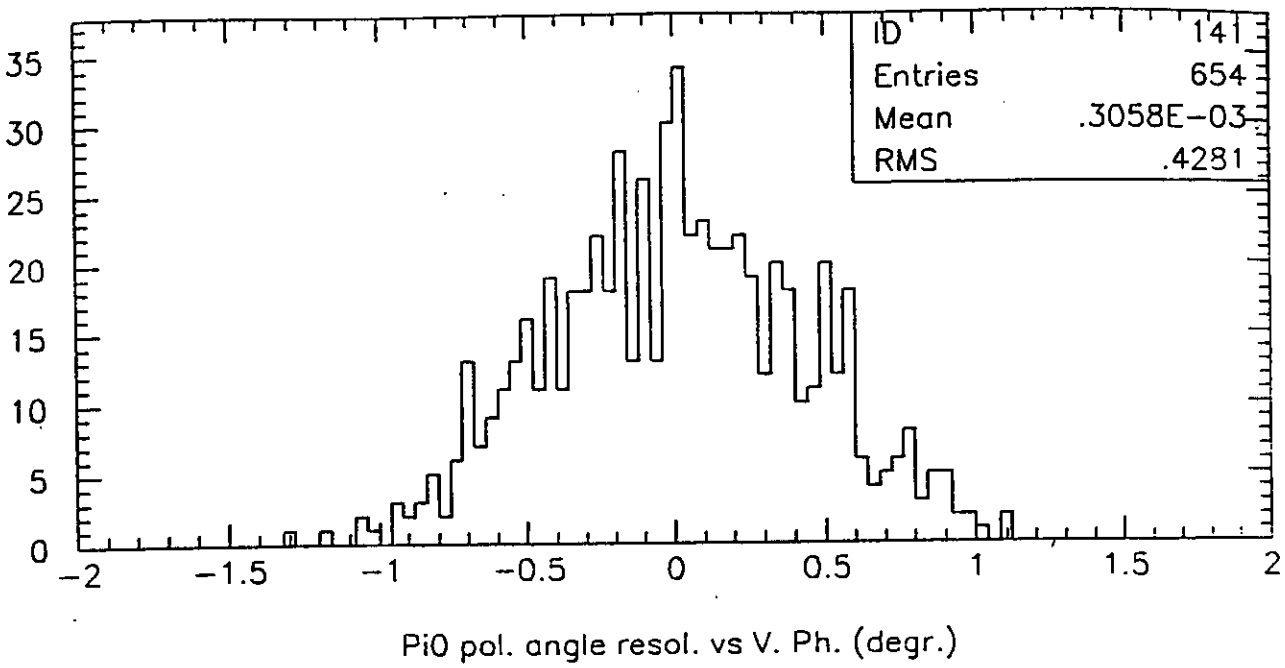

Figure 9. GEANT generated π^o angular resolution.

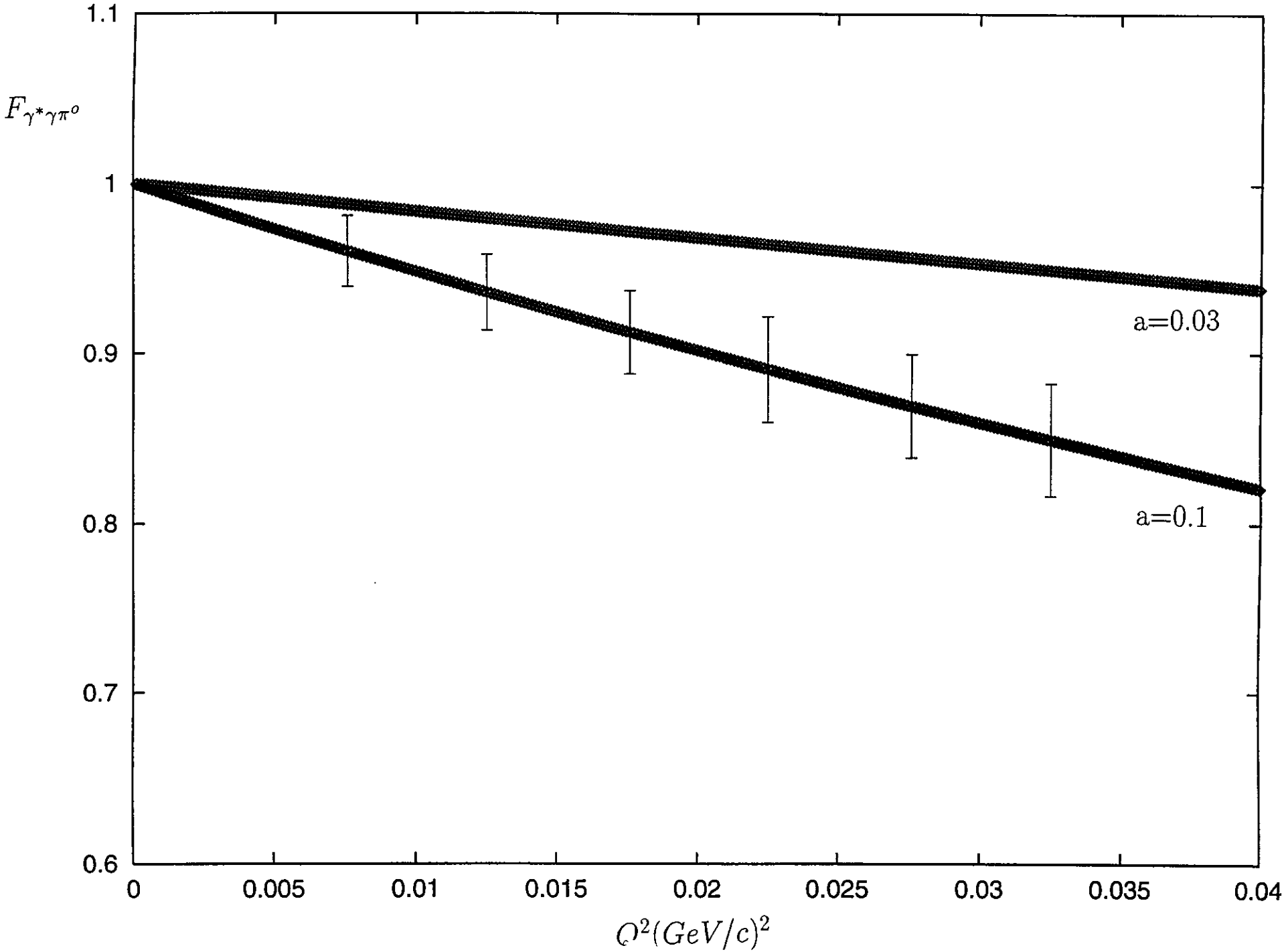
1.1
1
0.9
0.8
0.7
0.6
$F_{\gamma^*\gamma\pi^o}$
0
0.005
0.01
0.015
0.02
0.025
0.03
0.035
0.04
$Q^2(GeV/c)^2$
a=0.03
a=0.1

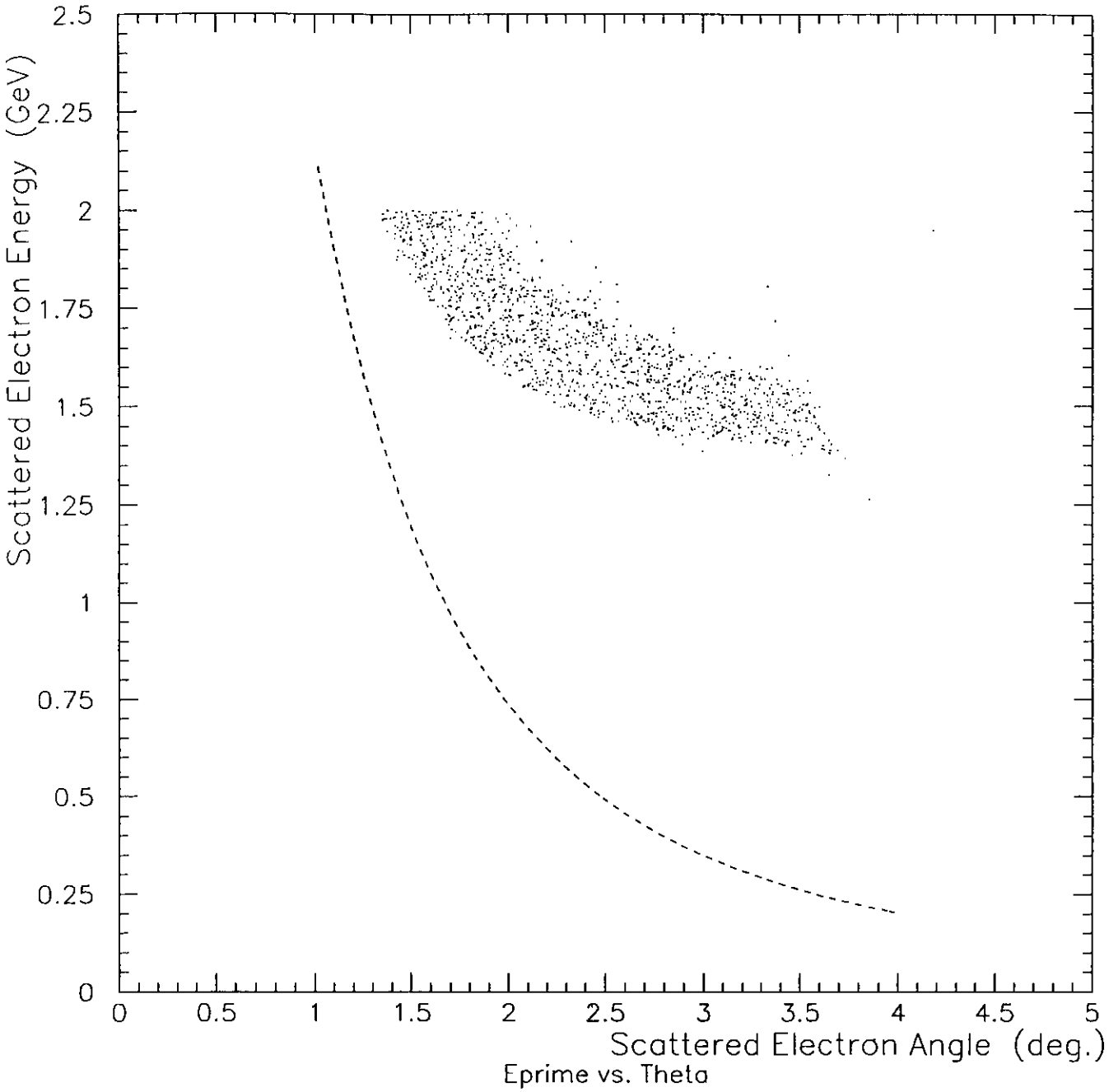

Figure 11. Shaded region: scattered electron energy and angle acceptance.
Dashed line: Möller scattering kinematics.

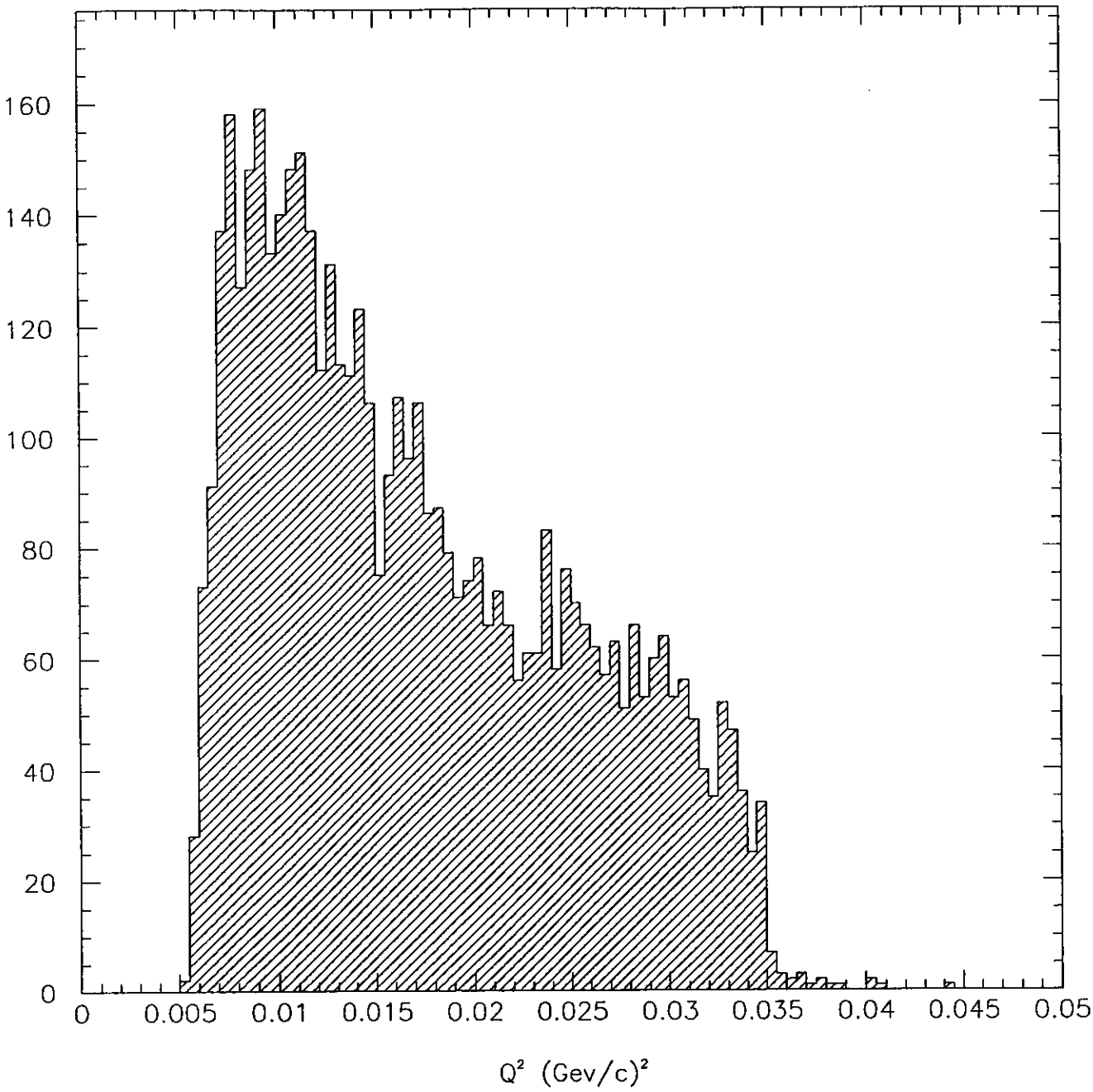

Figure 12. q_μ^2 phase space.

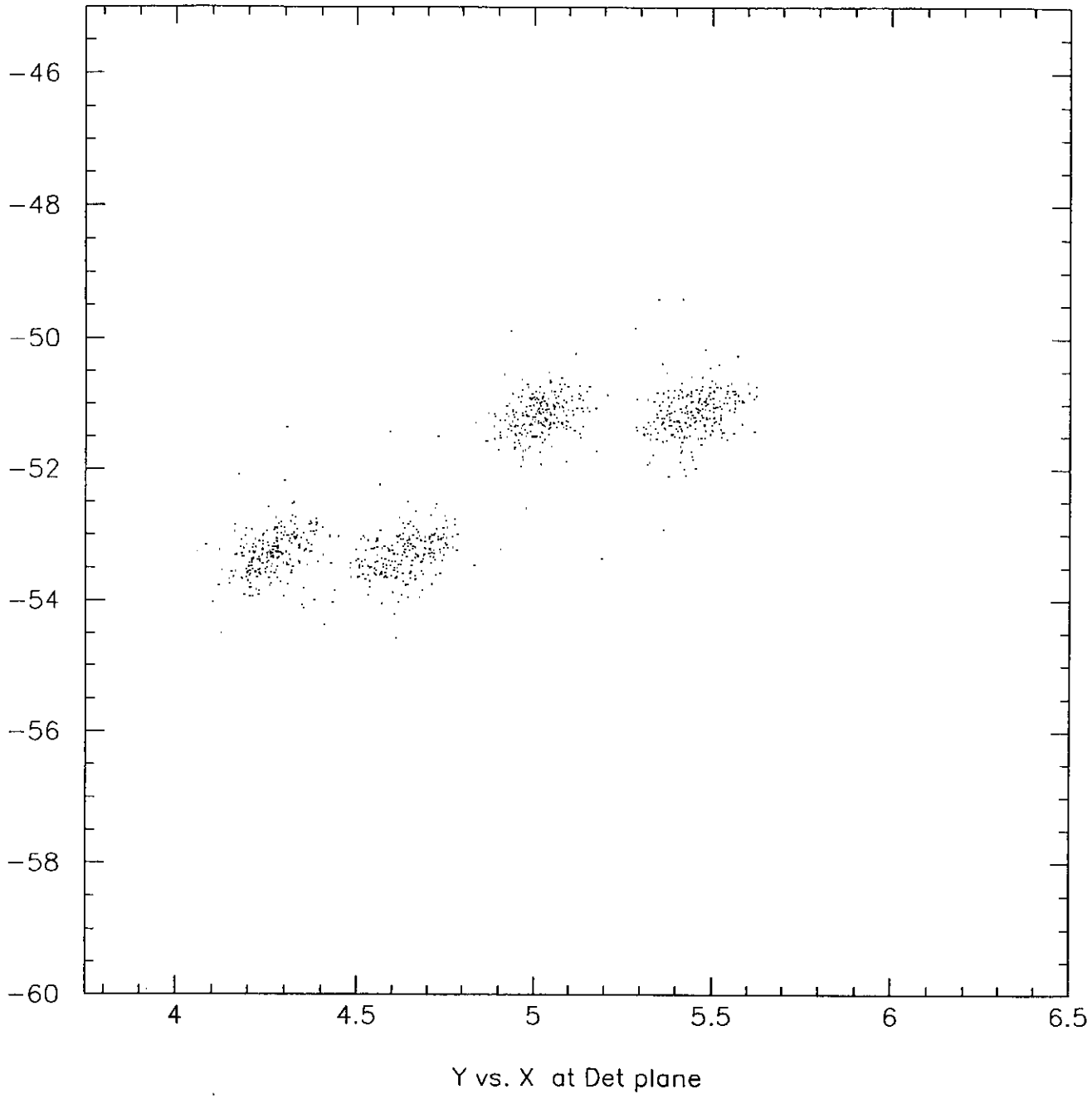

Figure 13. GEANT generated distribution of hit patterns of particles on the detector for two different energies and angles. Y axis is dispersive direction. Transverse displacements of hits are due to 2 mrad difference in scattering angle at the target.

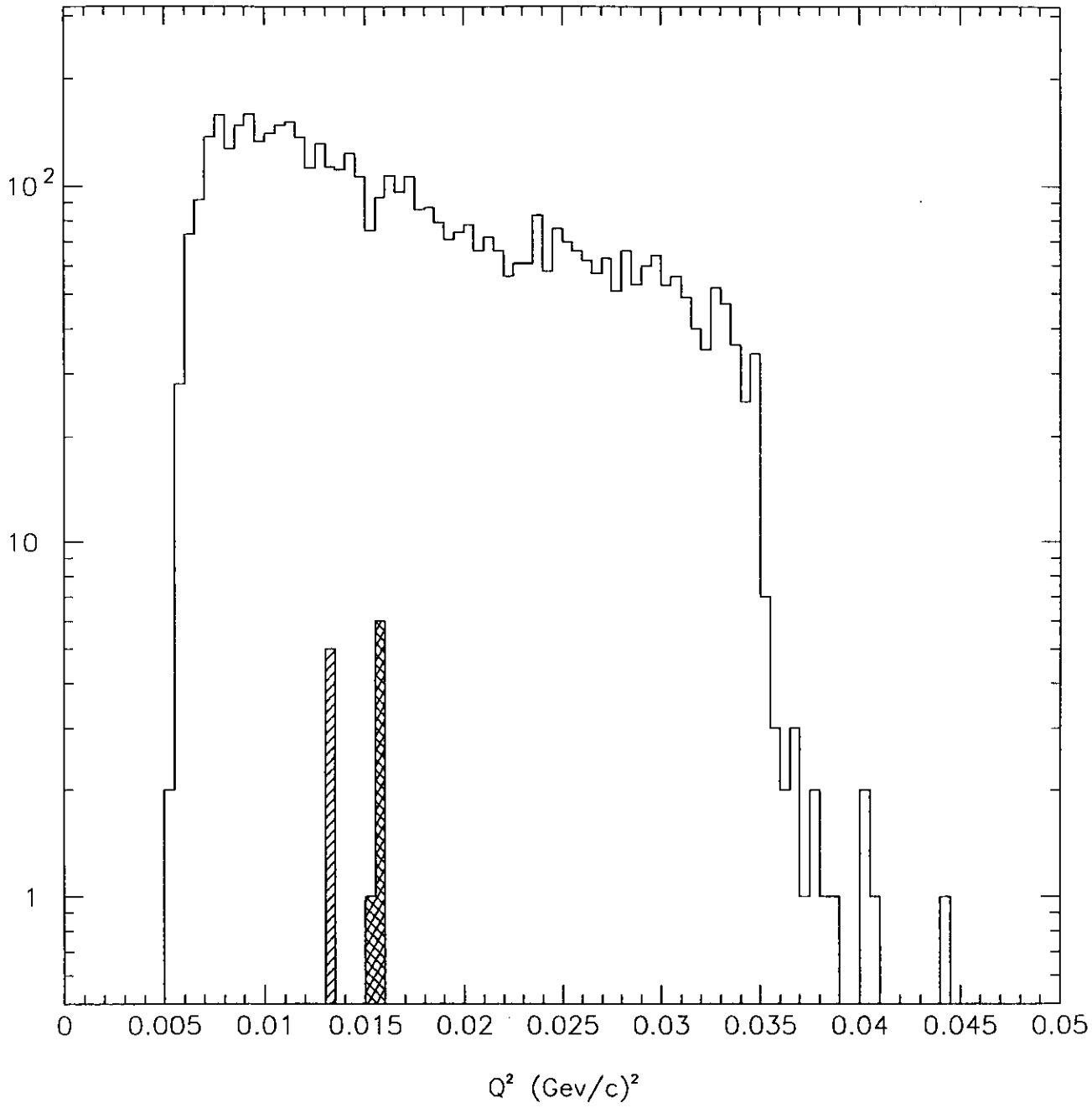

Figure 14. For a fixed energy, regions of q_μ^2 corresponding to the 2 mrad angular difference of the previous figure.

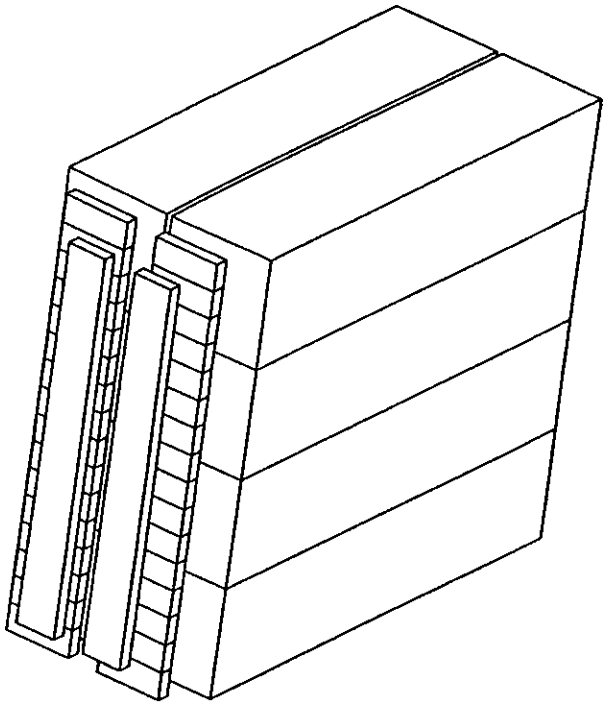

Figure 15. Conceptual design of present Möller polarimeter detector package containing aperture and hodoscope scintillators, and lead glass detectors.

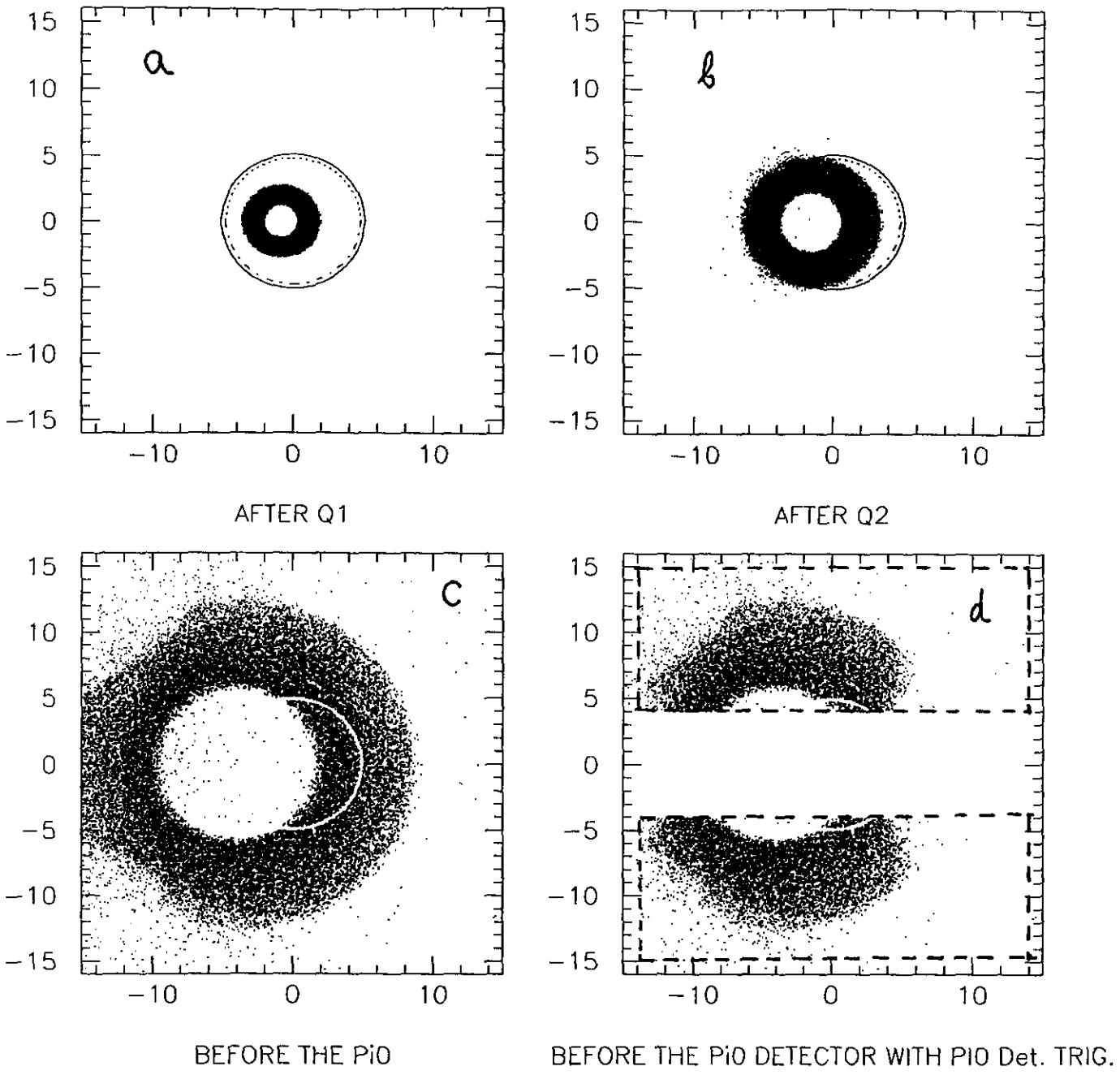

Figure 16. Spatial distribution of photon trajectories cut in planes perpendicular to the beamline (a) after the first quadrupole, (b) after the second quadrupole (c) before the lead glass pion detectors, and (d) before the lead glass pion detectors with an energy cut on the lead glass detector. Photons are sampled $90° \pm 20°$ in the center of mass. On (c) note the effect of the poles of the quadrupole. Dashed lines in (d) indicate position of lead glass detectors.